

## Open water production in Arctic sea ice: Satellite measurements and model parameterizations

H. L. Stern and D. A. Rothrock

Polar Science Center, University of Washington, Seattle

R. Kwok

Jet Propulsion Laboratory, California Institute of Technology, Pasadena

**Abstract.** Sequential synthetic aperture radar (SAR) images from the ERS 1 spacecraft were routinely used as input to the Geophysical Processor System at the Alaska SAR Facility from 1992 through 1994 to produce sea ice displacement vectors on a 5-km grid. We have combined some 5000 of these products, consisting of nearly 700,000 displacement vectors, into a set of 914 strips or mosaics of ice motion that span (mostly) 3-day intervals. For each strip we compute the opening and closing of leads based on the change in area of the 5-km grid cells. We also compute the area-averaged deformation or strain invariants of the motion. The small-scale (several kilometer) lead activity can be parameterized fairly well in terms of the large-scale (several hundred kilometer) strain invariants. Sea ice models implicitly contain such a parameterization through their constitutive equations. The well-known model of Hibler (1979) that uses a viscous-plastic rheology and an elliptical yield curve is in good agreement with our data. The variance in the data about this theoretical relationship is less than that suggested by a random model of sea ice motion. The data also indicate that shearing deformation contributes to the opening and closing of leads. Models with two categories or levels of ice thickness generally do not take shearing deformation into account in the evolution of the ice concentration, nor do they redistribute ice as a result of ridging. We show how to add these features to two-level models. However, we argue that three-level models consisting of open water, thin ice, and thick ice are much better suited to the proper treatment of open water production, and we present such a model.

### 1. Introduction

The Arctic sea ice cover is an insulating layer between the ocean and the atmosphere. The opening of cracks or leads in the ice creates areas of open water which significantly affect the air-ice-ocean interaction. In winter, newly opened leads are the source of new ice growth, brine rejection to the ocean, and rapid heat transfer from the ocean to the atmosphere. Although leads account for only a few percent of the surface area, their contribution to the area-averaged sensible heat flux is comparable to that of thick ice [Maykut, 1978], making the open water fraction an important parameter. When convergence of the pack ice forces leads to close, the thin ice in the leads is piled up into pressure ridges and forced down into keels, increasing the ice-ocean and ice-atmosphere drag. For these reasons, it is important to account separately for the positive and negative area changes in leads when considering the dynamics and thermodynamics of Arctic sea ice.

Five years ago, *Fily and Rothrock* [1990] addressed the problem of making measurements of the opening and closing of sea ice leads from a single pair of sequential synthetic aperture radar (SAR) images from the Seasat satellite. *Fily and Rothrock* [1990, p. 789] correctly predicted that “the next five years will produce a great quantity of high resolution imagery of sea ice, so we will proceed from a period of very little

detailed data about ice dynamics into an era of overwhelming amounts of data.” Their work was motivated by the question: “How will we analyze this imagery in a way that is relevant to large-scale sea ice models?” The emphasis of the paper was on an algorithm for computing the positive and negative changes in the area of leads in sea ice. In the present work we analyze measurements of lead opening and closing from 5000 pairs of SAR images. Our work is motivated by the question: What is the proper parameterization in large-scale sea ice models for the opening and closing of leads in terms of the ice deformation? We emphasize the scientific interpretation of the data, rather than the data analysis techniques.

Opening is defined as the fractional increase in area (relative to a whole image or scene) of those leads whose areas have increased; closing is the fractional decrease in area of those leads whose areas have decreased. The difference, opening minus closing, is the net fractional area change or divergence of the scene. Area changes are assumed to occur only in leads and not in multiyear ice. To measure these changes, an image is divided up into square cells 5 km on a side. The locations of all the cell corners are identified in a subsequent image of the same region acquired several days later. This ice tracking procedure and the resulting ice motion data are described in section 2. The change in lead area can then be computed either by counting the change in the number of lead pixels within each cell (using images classified by ice type) or simply by calculating the change in the area of each cell. A decrease in lead area may be due either to the closing of open water or to

Copyright 1995 by the American Geophysical Union.

Paper number 95JC02306.  
0148-0227/95/95JC-02306\$05.00

the ridging of thin ice; our measurements cannot distinguish between the two. The computation of lead area changes is discussed in section 3, along with the computation of the large-scale strain invariants.

The results presented in section 4 show that the opening and closing of leads depends on both the divergence and the shear in the ice pack. An ice cover that undergoes a pure shearing deformation produces 25% as much new open water as an ice cover that undergoes a purely divergent deformation of the same magnitude. Also, the variability or randomness in the relationship between lead activity and ice deformation is smaller than that suggested by a random model of sea ice motion [Thorndike, 1987]. Furthermore, this variability becomes even smaller as attention is restricted to the most "active" scenes, those that undergo the largest deformations. Therefore the opening and closing of leads can be parameterized reasonably well in terms of the large-scale ice deformation.

The plastic yield curve for pack ice has been related to lead activity through the energetics of the ridging process [Rothrock, 1975]. For a given yield curve this allows us to compute a theoretical relationship between lead activity and ice deformation, which we can compare with the data. In section 5 we show that the elliptical yield curve used by Hibler [1979] in the viscous-plastic rheology fits the data quite well. (There are other yield curves that also give a good fit.) This lends confidence to the rheology, but it does not imply that the production of open water is being treated properly; this must be done in a manner consistent with the thickness distribution theory of Thorndike *et al.* [1975], as shown in section 6.

Sea ice models attempt to predict the motion and thickness distribution of the ice. The thickness distribution evolves according to advection, ice growth and melt, and mechanical redistribution, in which ice of thickness zero (open water) is created by the opening of leads and thin ice is redistributed into thicker categories by ridging [Thorndike *et al.*, 1975]. The ice models used in most investigations incorporate a crude version of the thickness distribution in which there are just two categories or levels of ice thickness, thick ice and thin ice. The thick ice is described by its concentration, and the mass balance is maintained by an equation for the mean ice thickness. The most popular model of this variety is Hibler [1979]. More detailed formulations include Thorndike *et al.* [1975] with 10 levels; Hibler [1980] also with 10 levels; and Walsh and Zwally [1990], who base their model on Hibler [1979], but with three levels, although there is only one equation for the total ice concentration. More recently, Flato and Hibler [1995] have introduced a model with 28 levels that also distinguishes between ridged ice and level ice. In general, the two-level models (and the three-level model) allow open water production only through the divergence of the ice cover. Our data show that the shear in the ice cover also contributes to the production of open water. Two-level models that assign a thickness greater than zero to thin ice must redistribute some thin ice into thicker categories. In section 6 we show how to generalize the equation for ice concentration to take this redistribution into account. The extra term is a function of both the divergence and the shear in the ice cover, as well as the ice concentration. Hibler [1984] and Flato and Hibler [1991] included a similar term in their modified two-level models. The size of this term can be significant, depending on the assumptions about how much ice participates in ridging.

Some models incorporate a minimum lead fraction or max-

imum ice concentration as an ad hoc device to maintain a certain amount of open water in each grid cell at all times. Holland *et al.* [1993] and Chapman *et al.* [1994] have found that ice models are very sensitive to this minimum lead fraction. The effect of the new redistribution term is to create a small source of open water that may obviate the need for a minimum lead fraction parameter. Furthermore, under sustained convergence of the ice pack the new term prevents the ice concentration from exceeding unity. This situation was previously handled by capping the concentration at 1 and thickening the ice to conserve volume. Gray and Morland [1994] added a term on mathematical grounds to keep the concentration below 1, and they identified its asymptotic behavior. The new redistribution term derived here from the theory of Thorndike *et al.* [1975] accomplishes the same goal as Gray and Morland's term and shows that the original formulation of the dynamics of ice motion and deformation is capable of providing solutions to problems encountered in numerical implementations of the theory.

At the end of section 6 we introduce a three-level ice model (thick ice, thin ice, open water) that gives a more realistic accounting of open water production than two-level models but without the complication of a full thickness distribution. Conclusions are summarized in section 7.

At this point we would like to comment on the relationship between sea ice processes, data, and numerical models. The discontinuous, anisotropic behavior captured in Figure 1 is certainly not simulated by established ice models. Rather, models attempt to provide a spatially and temporally averaged description of real events. Even increasing the spatial resolution of a continuous, isotropic model of the Hibler [1979] type would not reproduce the observed behavior. Therefore the small-scale (5 km) data must be collected and averaged into large-scale (100 km) quantities for the purposes of comparison with model parameterizations. We use the small-scale information for aggregating local area changes into large-scale opening and closing of the pack ice and for computing an area-averaged measure of the ice deformation on the same (large) scale. Certainly the small-scale, detailed SAR data can be used to study the discrete nature of sea ice processes, such as velocity jumps and lead orientation, but comparisons with established models require appropriate averaging.

## 2. Ice Motion Products

The first European Remote Sensing Satellite (ERS 1) was launched in July 1991 into a Sun-synchronous orbit at 98.5° inclination, providing coverage of the Arctic up to 85°N latitude. In its first 2 years, ERS 1 provided 3-day repeat coverage of the Arctic during the exact 3-day repeat cycle and during the 35-day repeat cycle, when there was a drifting 3-day subcycle with considerable swath overlap at high latitudes. The SAR aboard ERS 1 images a swath 100 km wide at about 23° incidence angle. Data are collected and processed by various ground receiving stations around the world, including the Alaska SAR Facility (ASF) in Fairbanks. The ASF produces geocoded, low-resolution images, mapped to the special sensor microwave/imager (SSM/I) polar stereographic projection, that are 100 × 100 km in extent with a pixel size of 100 m.

The Geophysical Processor System (GPS) at ASF used these images as input to an automatic ice-tracking algorithm [Kwok *et al.*, 1990] and an automatic ice classification algorithm [Kwok *et al.*, 1992]. The tracking procedure begins with a pair of

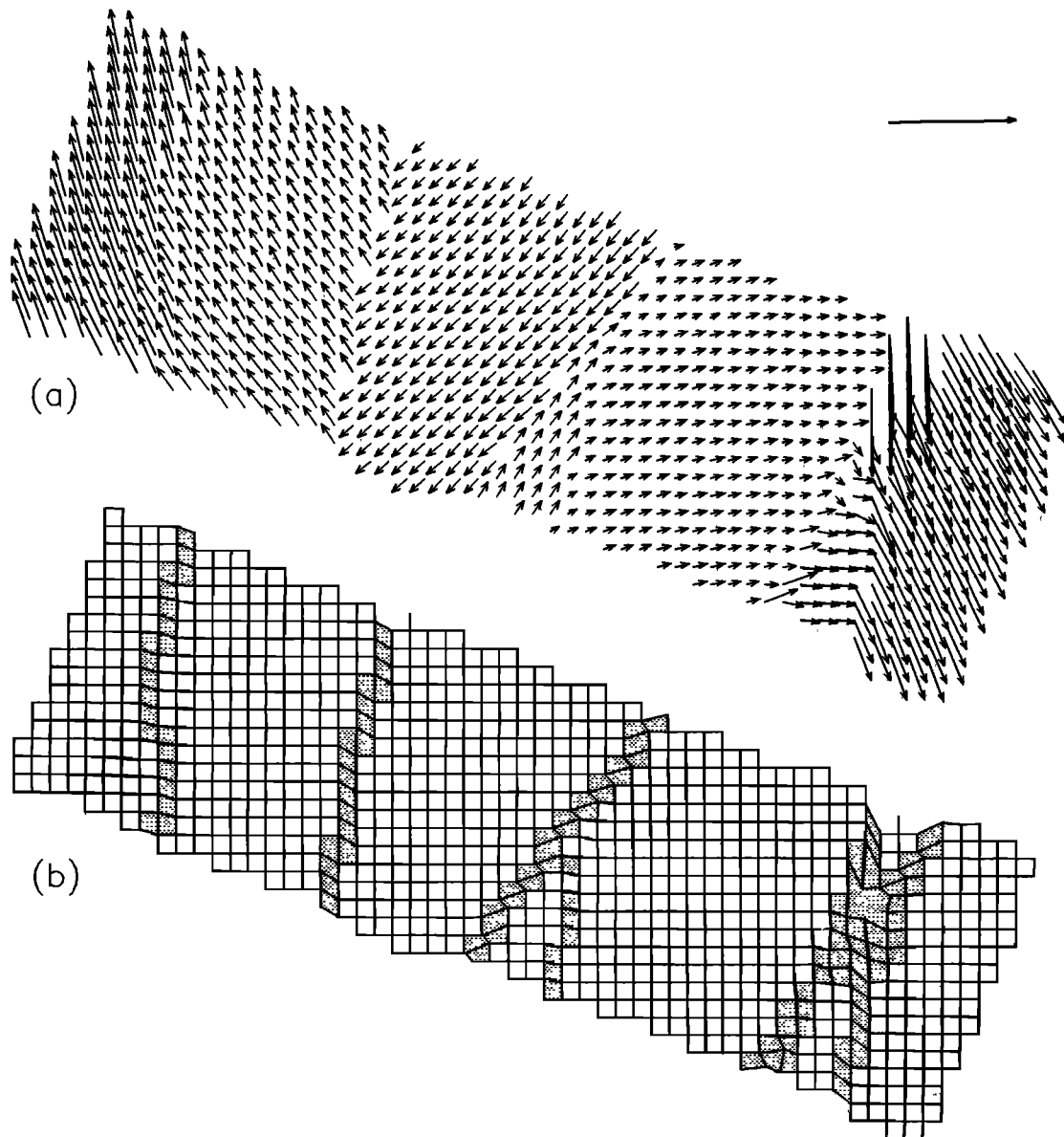


**Figure 1.** A mosaic of six ice motion products, with a total of 987 displacement vectors, showing the relative ice motion from March 22 to 25, 1992, at approximately  $178^{\circ}\text{W}$  between  $73^{\circ}\text{N}$  and  $75^{\circ}\text{N}$ . Northwest is to the right. (a) Deviations from the mean ice displacement, scaled up by a factor of 3. The mean displacement (about 12 km) is shown by the single vector at the top right (also scaled up by a factor of 3). The vector tails lie on a regular 5-km grid. There are clearly several regions of uniform motion separated by sharp discontinuities. (b) Configuration of the initially regular 5-km grid after 3 days. Most of the cells are rigid, with little or no deformation or area change. The cells with the greatest deformations are shaded.

images separated in time by (typically) 3 days and assigns a regular array of grid points with 5-km spacing to the first image. The algorithm attempts to track the ice at each grid point to its new location in the second image, using cross-correlation and feature-matching techniques. The result is a set of corresponding tie points or, equivalently, displacement vectors on a regular 5-km grid. One ice motion product contains, on average, more than 200 vectors or pairs of tie points.

The ice classification algorithm assigns each image pixel to one of four classes, using a maximum likelihood method and a look-up table of the expected mean and standard deviation of the backscatter of the four ice types. The classes are multiyear ice, first-year rough ice, first-year smooth ice, and new ice/open

water. The result is an image product in which each pixel contains one of four possible numbers that represents the appropriate ice type for that pixel.

Initially, we envisioned using the ice motion and ice type products together to compute the opening and closing of leads. In the end we used only the ice motion products, for reasons given in section 3. We combined the individual ice motion products into strips or mosaics up to 500 km long. Since lead systems extend for hundreds of kilometers, as seen, for example, in advanced very high resolution radiometer (AVHRR) images, the purpose of the mosaicking was to match the scale of analysis with the scale of the physical processes. Each mosaic covers about the same area as several grid cells of a typical

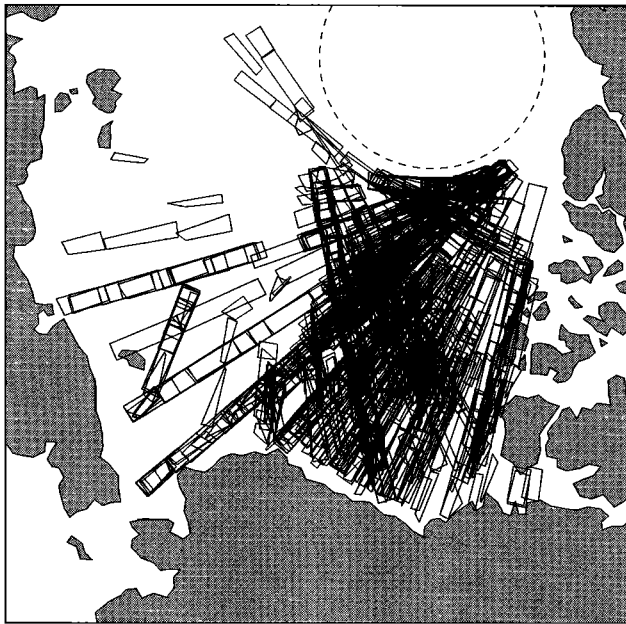


**Figure 2.** A map showing the locations of the 914 strips or mosaics of ice motion data. Alaska is at the bottom; the dashed circle at the top is 85°N, the approximate northern limit of satellite coverage.

sea ice model. The mosaicking procedure involves several steps: identifying adjacent products, locating and removing erroneous displacement vectors, combining the data sets, and eliminating duplicate or overlapping data. By applying these steps to approximately 5000 ice motion products, we created a new data set consisting of 914 strips that contain nearly 700,000 individual displacement vectors. An example of such a strip is shown in Figure 1. Figure 1a shows the deviations from the mean ice displacement over a 3-day period (scaled up by a factor of 3), and Figure 1b shows how the initially regular 5-km grid has deformed after 3 days.

The spatial coverage of the 914 strips is shown in Figure 2. The data cover the Beaufort Sea and the western Arctic Ocean up to 85°N latitude. The temporal coverage extends from the fall of 1991 through the fall of 1992. In 93% of the strips the time interval spanned by the ice displacement is 3 days. The other 7% of the data span intervals of 6, 9, 12, and 15 days.

We note that the analysis in this paper does not use SAR images directly; it uses geophysical products (ice motion) derived automatically from 10,000 SAR images. This represents a reduction in data volume by a factor of about 230 over the geocoded low-resolution images or a factor of 6400 over the full-resolution images. We strongly believe that automated geophysical processing systems are the only reasonable way to analyze the enormous amounts of satellite data now being collected.

### 3. Computation of Opening, Closing, and Deformation

#### 3.1. Area Change in Leads

*Fily and Rothrock* [1990] presented two methods for computing the area change in leads, with several variations on each

method. The first method (called “lead area”) requires both ice motion data and ice type data, such as those produced by the GPS. The algorithm first counts the number of lead pixels in a grid cell, which are those pixels labeled new ice/open water by the GPS classification algorithm. The ice motion data give the new locations of the cell corners in the subsequent image, and the lead pixels in the same (possibly deformed) cell are counted again. An increase in the number of lead pixels contributes to the opening; a decrease contributes to the closing. The second method (called “cell area”) requires only ice motion data. The area change of each entire cell is computed; positive changes contribute to opening, negative changes to closing.

We compared opening and closing measurements taken from 49 pairs of images, using the lead area method versus the cell area method. *Fily and Rothrock* [1990] found the lead area method to be more accurate, and we know that the cell area method overestimates the opening and closing. Cells on a rigid piece of ice should not change area, but a small error in the location of a tie point causes small area changes in the four surrounding cells. These area changes do not cancel, since increases and decreases are summed separately. The lead area method is less sensitive to tie point errors. Nevertheless, we found a high correlation (0.89) between the opening and closing computed by one is a good predictor of the trend computed by the other. Although *Fily and Rothrock* used the lead area method in their analysis of a single image pair, we use the cell area method for the following reasons.

1. The GPS ice classification procedure introduces unknown errors into the results. Thin ice in leads can be misclassified as multiyear ice due to frost flowers on the surface that increase the radar backscatter. Open water in leads can also be misclassified as multiyear ice due to wind roughening of the surface. Furthermore, the area occupied by pixels classified as new ice/open water is usually small, making the relative area change especially sensitive to errors in the classification. *Fetterer et al.* [1994] examined the performance of the ice classification algorithm, but they did not evaluate the accuracy of the new ice/open water class because of the small sample sizes in the 68 images they analyzed.

2. As previously noted, the difference of opening and closing (denoted  $D$ ) is the net fractional area change or divergence of a scene. We compute the divergence independently, using the ice motion data, as described in section 3.2, and this provides a consistency check against  $D$ . However, this computed divergence only explains 70% of the variance in  $D$  for the lead area method, whereas it explains 99% of the variance in  $D$  for the cell area method. The error in the computed divergence is small, so the inconsistency in the lead area method must arise in the calculation of the opening and closing, possibly from errors in the GPS ice classification, or because moving cell boundaries that are not material boundaries can cause lead pixels to shift from one cell to another.

3. The cell area method is computationally simpler than the lead area method and does not require storing and processing image-type data (i.e., the classified SAR images). This reduces the input data volume from about 20 gigabytes to 100 megabytes.

Let us examine in more detail the errors in the calculation of the opening and closing. From now on we use the cell area method. Figure 3 shows the histogram of the computed opening and closing for the 914 strips of data. We want to answer

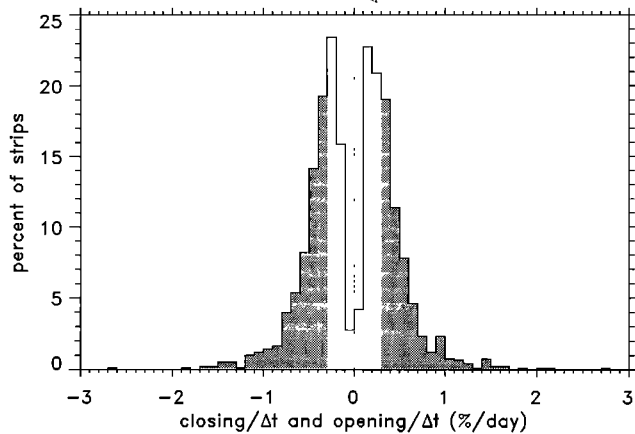


**Figure 3.** Histogram of the rates of opening and closing for all 914 strips of data. Closing values are displayed as negative numbers. The area under the histogram is 200%, because each strip contributes one opening value and one closing value. The shaded region highlights the values above the minimum level of significance of 0.3% per day.

the question: What level of opening and closing is significant? In other words, how much opening and closing could be spuriously generated by motion that is nearly rigid, in which there is no real lead activity? To answer this question, we identified the most rigid strips of data, as determined by the statistics of the tie point displacements  $(u_i, v_i)$ . The variability in  $u_i$  (and  $v_i$ ) for each strip can be measured by the range  $R_u = \max(u_i) - \min(u_i)$  or by the standard deviation  $\sigma_u$ . There are 14 strips of data for which both  $R_u$  and  $R_v$  are less than 500 m. In these strips the largest values of  $\sigma_u$  and  $\sigma_v$  are 100 m. (Recall that the pixel size in the images is 100 m.) Therefore these strips undergo almost pure translation, with no rotation or deformation. We find that the largest value of the opening is 0.005, and the largest value of the closing is 0.007. Visual inspection of these and other strips confirms that values of opening and closing smaller than about 0.008 cannot be regarded as meaningful. Such small fractional area changes can be completely accounted for by small random tie point errors. This is consistent with our numerical simulations of tie point motion, which show that random Gaussian displacements with a standard deviation of 100 m typically induce opening and closing values of about 0.008. Note that the time interval over which the motion occurs does not enter into the error analysis, which is concerned only with the relative change between the initial and final tie point configurations. Since 93% of the scenes represented in Figure 3 are derived from 3-day displacement fields, the minimum level of significance for opening and closing (0.008) is approximately equivalent to 0.003 per day for these data. The shaded region in Figure 3 highlights the values above this threshold.

### 3.2. Deformation

Deformation is embodied in the strain tensor  $\varepsilon$ , whose elements are composed of the spatial derivatives of the displacement field. Let  $(x, y)$  represent position and  $(u, v)$  represent displacement. We wish to compute the area-averaged value of  $\partial u/\partial x$  (and the other three partial derivatives) for each strip of ice motion data. Let  $A$  denote the total area over which the average is taken, and let  $u_x$  denote the average value. Then

$$u_x = \frac{1}{A} \iint \frac{\partial u}{\partial x} dx dy = \frac{1}{A} \oint u dy \quad (1)$$

where the first equation is simply the definition of the area average and the second equation follows from the divergence theorem, the integral being taken around the boundary of the region. We compute  $u_x$  by constructing a finite difference approximation to  $\partial u/\partial x$  for each cell and averaging over all cells. This is the discrete analog of the first equation in (1). It turns out, not surprisingly, that the contributions from all the interior grid points cancel, leaving an expression equivalent to the discrete version of the contour integral in (1). The other partial derivatives  $(u_y, v_x, v_y)$  are computed in the same way as  $u_x$ .

Thorndike [1986] presented the above method and discussed the question of the existence and interpretation of the derivatives. Apparently  $u$  is a discontinuous field (see Figure 1) and its spatial derivatives may not exist along zones of deformation. However, the jumps in  $u$  are all finite, and the contour integral in (1) is well defined, even if  $\partial u/\partial x$  does not exist in the limit as the grid spacing goes to zero. The computed value of  $u_x$  from the contour integral in (1) does depend on the grid spacing, but since  $u$  is approximately a piecewise linear function which is very well resolved by the current grid spacing of 5 km, the discretization error is small. A denser sampling of  $u$  would not change  $u_x$  by much. The net result is that these area-averaged derivatives are meaningful quantities that characterize spatial changes in the displacement field in an average or large-scale sense, even though that field may have finite jumps.

The area-averaged derivatives are combined to form two large-scale strain invariants:

$$\text{divergence} = \varepsilon_I = u_x + v_y \quad (2)$$

$$\text{shear} = \varepsilon_{II} = \sqrt{(u_x - v_y)^2 + (u_y + v_x)^2}$$

which are the sum and difference of the principal values of  $\varepsilon$ . Alternatively, the polar form of these invariants may be used:

$$|\varepsilon| = \sqrt{\varepsilon_I^2 + \varepsilon_{II}^2} \quad \theta = \arctan(\varepsilon_{II}/\varepsilon_I). \quad (3)$$

The quantity  $|\varepsilon|$  is the magnitude of the deformation, and  $\theta$  indicates the relative contributions of divergence and shear: pure divergence ( $\theta = 0^\circ$ ), uniaxial extension ( $\theta = 45^\circ$ ), pure shear ( $\theta = 90^\circ$ ), uniaxial compression ( $\theta = 135^\circ$ ), and pure convergence ( $\theta = 180^\circ$ ). The quantities  $\varepsilon_I$ ,  $\varepsilon_{II}$ ,  $|\varepsilon|$ , and  $\theta$  are all dimensionless. We can divide the first three by the time interval  $\Delta t$  over which the displacements  $(u, v)$  occur to obtain the rates of divergence, shear, and deformation. Figure 4 shows histograms of these rates and of  $\theta$  for all 914 strips of data. The histograms can be approximated fairly well by Gaussian distributions, as shown.

Small tie point errors propagate into the calculation of  $u_x$  and the other derivatives and hence into the strain invariants. However, unlike the errors in opening and closing, which are always biased toward larger magnitudes, the contributions to the error in  $u_x$  can cancel. Therefore the strain invariants are less sensitive to tie point errors, and they can be determined more accurately. Considering the 14 strips of data whose motion is almost perfectly rigid, as described at the end of section 3.1, we find that the largest value of  $|\varepsilon|$  is 0.003. We adopt this figure as the level of significance or error estimate in the calculation of  $|\varepsilon|$ .

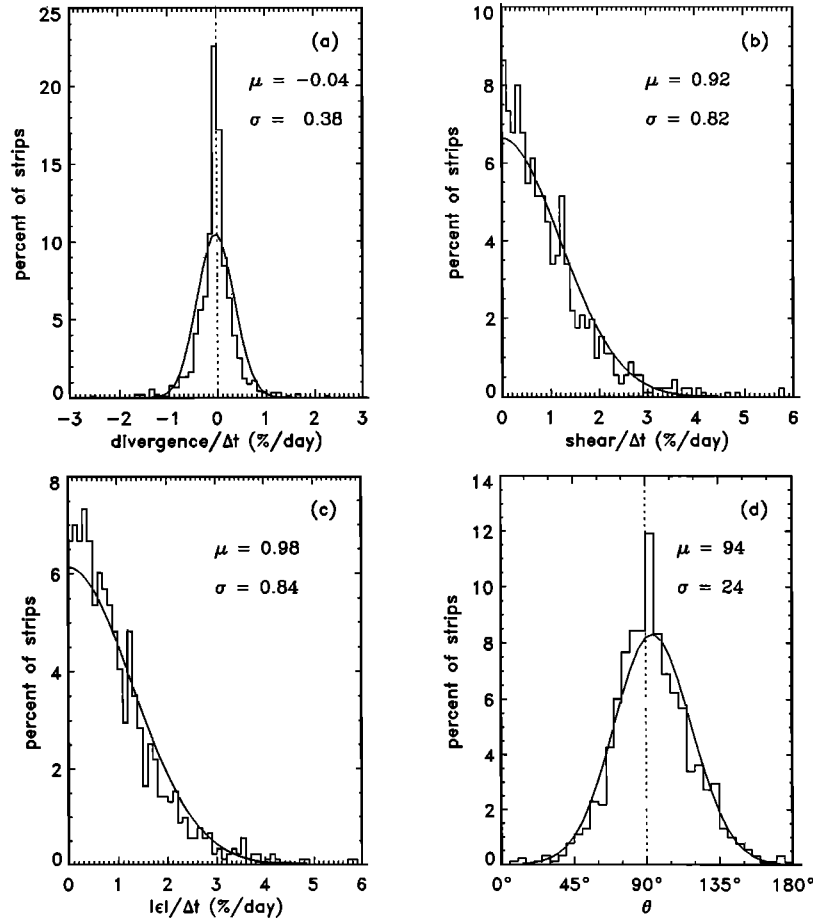


**Figure 4.** Histograms of the strain rate invariants from 914 strips of data: (a) divergence; (b) shear; (c)  $|\epsilon|$ , which is a measure of the magnitude of deformation; and (d)  $\theta$ , which is a measure of the relative contributions of divergence and shear. The mean  $\mu$  and standard deviation  $\sigma$  are included. The curves in Figures 4a and 4d are the Gaussian distributions with the same mean and standard deviation as the data. The curves in Figures 4b and 4c are the positive halves of the Gaussian distributions with mean 0 and variance  $\mu^2 + \sigma^2$ .

#### 4. Analysis and Results

The parameterization of lead opening and closing in terms of ice deformation was first presented by *Thorndike et al.* [1975]. The opening and closing were postulated to be directly proportional to the strain  $|\epsilon|$ , with the multiplier being a function of the type of deformation via  $\theta$ :

$$\text{opening} = |\epsilon| \alpha_o(\theta) \quad \text{closing} = |\epsilon| \alpha_r(\theta) \quad (4)$$

where  $\alpha_o(\theta) - \alpha_r(\theta) = \cos \theta$  in order that the difference of the opening and closing gives the divergence  $\epsilon_v$ . Since we have computed values of opening, closing,  $|\epsilon|$ , and  $\theta$  for each strip of ice motion data, we can examine the functions  $\alpha_r(\theta)$  and  $\alpha_o(\theta)$  empirically by plotting  $(\text{opening})/|\epsilon|$  versus  $\theta$  and  $(\text{closing})/|\epsilon|$  versus  $\theta$ . The fraction  $(\text{opening})/|\epsilon|$  is very sensitive to errors in  $|\epsilon|$  when  $|\epsilon|$  is small, so we impose a minimum cutoff value on  $|\epsilon|$  in order to restrict the error. Let  $\delta = \pm 0.003$  be the error in the estimate of  $|\epsilon|$ , as discussed in section 3.2. Ignoring for the moment the error in the opening, we have

$$\frac{\text{opening}}{|\epsilon| + \delta} = \left( \frac{\text{opening}}{|\epsilon|} \right) \left( \frac{1}{1 + \delta/|\epsilon|} \right) = \left( \frac{\text{opening}}{|\epsilon|} \right) f \quad (5)$$

where the first factor on the right is the true value and the second factor  $f$  is the error. If we require  $0.9 < f < 1.1$ , then

this implies  $|\epsilon| > 0.03$ . This restriction has the effect of screening out those strips of data for which there is not much ‘‘action.’’ This is exactly our intent anyway; we only want to examine the relation (4) when the ‘‘signal’’ (lead activity) is strong relative to the ‘‘noise’’ (uncertainties in computed values).

Now let  $\gamma = 0.008$  be the error in the estimate of the opening, as discussed in section 3.1. Then  $\gamma/|\epsilon|$  is the error in  $(\text{opening})/|\epsilon|$ , and it is no larger than  $0.008/0.03 = 0.27$ . With the additional 10% error due to the factor  $f$  in (5) the total estimation error in  $(\text{opening})/|\epsilon|$  is no larger than 0.3 for the restricted set of data in which  $|\epsilon| > 0.03$ . Furthermore, as we narrow our attention to the more active displacement fields by increasing the cutoff threshold for  $|\epsilon|$  above 0.03, the estimation error decreases. The size of this error will become more meaningful shortly when we look at the variability in  $(\text{opening})/|\epsilon|$  itself.

Figure 5 shows  $(\text{opening})/|\epsilon|$  and  $(\text{closing})/|\epsilon|$  versus  $\theta$  using data from the 342 strips for which  $|\epsilon| > 0.03$  and for which the time interval  $\Delta t$  of the ice motion is 3 days. The data have been grouped into  $5^\circ$  bins of  $\theta$ , and the mean for each bin is plotted as a solid dot. A single standard deviation has been calculated from all the deviations of the data around these means. This standard deviation (0.09) is plotted as a bar above and below

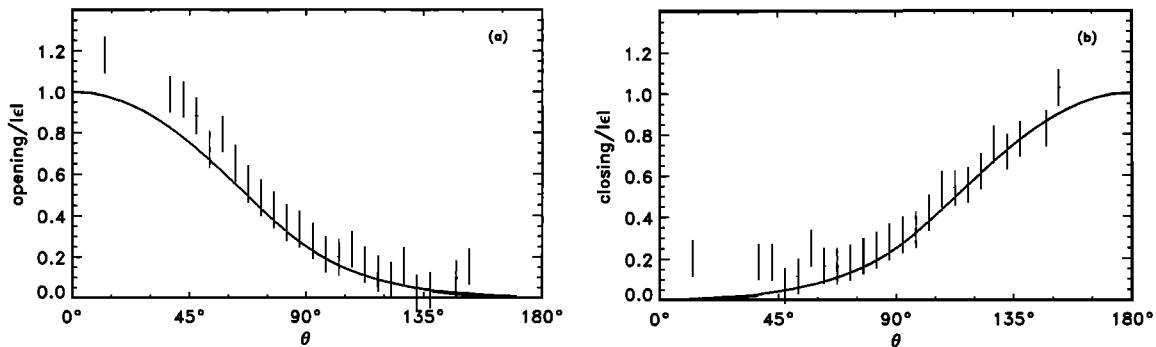


**Figure 5.** (a) Opening/ $|\varepsilon|$  and (b) closing/ $|\varepsilon|$  versus  $\theta$ , using data from the 342 strips for which  $|\varepsilon| > 0.03$  and for which the time interval  $\Delta t$  of the ice motion is 3 days. The data have been grouped into  $5^\circ$  bins of  $\theta$ , and the mean for each bin is plotted as a solid dot. A single standard deviation has been calculated from all the deviations of the data around the appropriate means. This standard deviation (0.09) is plotted as a bar above and below the mean values. We note that 98% of these data lie in the range  $45^\circ < \theta < 135^\circ$ , with only 1% in each tail of  $\theta$ ; pure divergence or convergence is very rare. The curves that pass near the data are derived from the elliptical yield curve for pack ice used by Hibler [1979]. The outlier at  $\theta = 12^\circ$ , which comes from a single strip of data, appears to be due to tie point errors that boost the opening and closing values without affecting  $|\varepsilon|$  much.

the mean values. We note that 98% of the data lie in the range  $45^\circ < \theta < 135^\circ$ , with only 1% in each tail of  $\theta$ ; pure divergence or convergence is very rare. The curves that pass near the data are derived from the elliptical yield curve for pack ice used by Hibler [1979] and will be explained in section 5. Fily and Rothrock [1990, Figure 9] show a figure similar to our Figure 5, but theirs contains only five data points. Now that we have hundreds of data points, the tight relationship between lead opening and ice deformation is more apparent. This relationship holds equally well regardless of the season or the length of the strip of data, which varies from about 100 to 500 km. Notice that even in pure shear ( $\theta = 90^\circ$ ) the ratio of opening to  $|\varepsilon|$  is about 25%.

Thorndike [1987] developed a model of sea ice motion in which leads are randomly positioned according to a Poisson distribution and the velocity discontinuities across leads have a Gaussian distribution. He used this Poisson-Gauss (PG) model to compute the opening of leads and the ice deformation. He found that for a given range of  $\theta$  the distribution of (opening)/ $|\varepsilon|$  is quite broad. We compare the distribution of (opening)/ $|\varepsilon|$  in the data for the range  $85^\circ < \theta < 95^\circ$  to Thorndike's [1987, Figure 3, curve b] distribution for the case of pure shear. The results are summarized in Table 1. The first line is the PG model, and the numbers in the three rightmost columns are estimated from Thorndike's figure. The remaining three lines in Table 1 are derived from our data, using only those scenes for which  $|\varepsilon|$  is greater than the given threshold.

Comparing the PG model to the data with no restrictions on  $|\varepsilon|$  (first two lines of the table), we see that the two distributions of (opening)/ $|\varepsilon|$  have about the same maximum values (6 and 5.7), but the peak of the data distribution is at a much smaller value (0.25) than that of the PG distribution (1.8), and the shape of the peak is much sharper and narrower for the data (0.4) than for the PG model (2). Looking at the third line of Table 1, we see that by eliminating the four scenes with the smallest values of  $|\varepsilon|$ , which are smaller than the measurement error in  $|\varepsilon|$ , the maximum value of (opening)/ $|\varepsilon|$  is reduced by a factor of 2. The tail of the distribution is extremely thin. A further restriction on  $|\varepsilon|$  that eliminates half of the scenes (fourth line of Table 1) sharpens the distribution by a factor of

2 and drastically reduces the maximum value without shifting the location of the peak. All of this implies that if the relationship between lead activity and ice deformation is considered to be the result of a random process, then that process has a small variance and that variance decreases as the magnitude of the ice deformation increases.

## 5. Plastic Rheology of Sea Ice

The momentum equation for sea ice contains a term for the internal ice stress, and this depends on the strain rates via the constitutive equations, which embody the material properties of the ice. One possible constitutive relation for sea ice is the viscous-plastic formulation used by Hibler [1979] in his dynamic thermodynamic model, in which the ice behaves like a viscous fluid at very small strain rates and like a plastic material at normal strain rates. The stress-strain rate relationship can be written very simply as

$$\sigma_I = \zeta \dot{\varepsilon}_I - P/2 \quad \sigma_{II} = \eta \dot{\varepsilon}_{II} \quad (6)$$

where  $\sigma_I$  is the compressive stress,  $\zeta$  is the bulk viscosity,  $\sigma_{II}$  is the shear stress,  $\eta$  is the shear viscosity,  $P$  is the compressive

**Table 1.** Properties of the Distribution of (Opening)/ $|\varepsilon|$  for Shearing Deformations, Computed From the Poisson-Gauss Model and From Our Data, With Various Thresholds of  $|\varepsilon|$ , Below Which Data Are Not Used

Case	$ \varepsilon $ Threshold	Number of Scenes	Maximum Value	Peak Location	Width at Half-Peak Height
PG	0	many	6	1.8	2
Data	0	186	5.7	0.25	0.4
Data	0.003	182	2.9	0.25	0.4
Data	0.03	89	0.74	0.25	0.2

Here  $|\varepsilon|$  is the magnitude of deformation, PG is the Poisson-Gauss model, and "data" refers to this paper. The measurement error in  $|\varepsilon|$  is estimated at 0.003. The distributions derived from our data are much narrower than that of the Poisson-Gauss model.

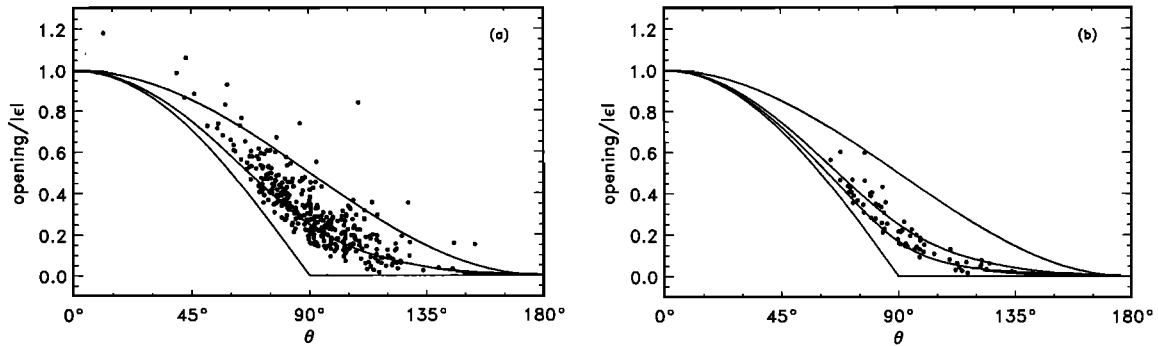


**Figure 6.** (a) The same data as in Figure 5a, but without grouping the data into bins of  $\theta$ . Each strip of ice motion data generates one point. The three curves correspond to the functions  $\alpha_o(\theta)$  derived from the elliptical yield curve with aspect ratios  $e = 1$  (top [Thorndike et al., 1975]),  $e = 2$  (middle [Hibler, 1979]), and  $e = \infty$  (bottom [Flato and Hibler, 1992]). (b) Similar to Figure 6a, but the threshold on  $|\varepsilon|$  has been raised to 0.07, leaving data from the 67 most active scenes. The four curves correspond to (from top to bottom)  $e = 1, 2, 3,$  and  $\infty$ .

strength of the ice, and  $\dot{\varepsilon}_I$  and  $\dot{\varepsilon}_{II}$  are the divergence and shear of the velocity field. (The “dot” distinguishes them from the divergence and shear of the displacement field, as in section 3.2.) The viscosities  $\zeta$  and  $\eta$  are chosen such that plastic failure occurs when the state of stress lies on the elliptical yield curve

$$\frac{(\sigma_1 + P/2)^2}{(P/2)^2} + \frac{(\sigma_{II})^2}{(P/2e)^2} = 1 \quad (7)$$

where  $e$  is the ratio of the major axis to the minor axis and, additionally,  $\eta = \zeta/e^2$ . Hibler [1979] used  $e = 2$ , and Thorndike et al. [1975] implicitly assumed  $e = 1$  (a circle). In the limit as  $e \rightarrow \infty$ , the ellipse becomes flattened into a line segment; this is the cavitating fluid rheology [Flato and Hibler, 1992], in which the ice does not resist shearing ( $\eta = 0$ ) or divergence but does resist convergence.

Rothrock [1975] showed how to associate a yield curve with the function  $\alpha_r(\theta)$  that describes ridging. The appropriate function associated with the yield curve (7) is

$$\alpha_r(\theta) = -\frac{1}{2} \cos \theta + \frac{1}{2} \sqrt{(\cos^2 \theta) + (\sin^2 \theta)/e^2} \quad (8)$$

and the function that describes opening is  $\alpha_o(\theta) = \cos \theta + \alpha_r(\theta)$ . These functions are plotted in Figure 5 for the case  $e = 2$ . The data used in Figure 5 for  $(\text{opening})/|\varepsilon|$  are plotted in full in Figure 6a, without grouping them into bins of  $\theta$ . In addition, the three functions  $\alpha_o(\theta)$  corresponding to the three cases  $e = 1$  (top curve),  $e = 2$  (middle curve), and  $e = \infty$  (bottom curve) are also plotted. Recall that these data are restricted to the 342 strips (out of the 848 strips with  $\Delta t = 3$  days) in which  $|\varepsilon| > 0.03$  in order to keep the error in  $(\text{opening})/|\varepsilon|$  from dominating the signal.

Figure 6b is similar to Figure 6a, but the threshold on  $|\varepsilon|$  has been raised to 0.07, leaving the 67 most active strips. Four curves are plotted in Figure 6b, corresponding to  $e = 1, 2, 3,$  and  $\infty$ . Figures 5 and 6 show that there is good agreement between the data and the opening implied by the elliptical yield curve with  $e = 2$ . This lends a degree of confidence to the plastic rheology, but two important points must be noted. First, other yield curves besides the ellipse can give a good fit to the data. For example, the “parabolic lens” [Rothrock, 1975] gives rise to a function  $\alpha_r(\theta)$  that is nearly the same as that generated by the ellipse with  $e = 2$ . The ellipse and the parabolic lens imply different plastic behavior of the ice in divergence and conver-

gence, but the data do not allow us to distinguish between the two yield curves. The second important point is that although the rheology in an ice model may give rise to an “opening” curve that agrees with the “opening” data (as in Figures 5 and 6), the model may not necessarily treat open water production consistently in its equation for ice concentration. We discuss this more fully in section 6.

The cavitating fluid rheology is thought to be appropriate for large-scale climate studies with monthly averaged forcing fields, rather than daily fields [Flato and Hibler, 1992]. Most of our ice motion data are for time intervals  $\Delta t$  of 3 days, but some of the data spans intervals of 6, 9, 12, and 15 days. The shape of the theoretical opening curve  $\alpha_o(\theta)$  derived from the elliptical yield curve depends on the parameter  $e$ , the aspect ratio of the ellipse. In an effort to test the cavitating fluid approximation, we computed the values of  $e$  that give the best fit of  $\alpha_o(\theta)$  to the data for different intervals  $\Delta t$ , but there is no apparent trend in  $e$  with increasing  $\Delta t$ . Instead, we find an increasing trend in  $e$  as  $|\varepsilon|$  increases, with  $e$  leveling off just above 2 for  $|\varepsilon| > 0.05$ . Of course,  $|\varepsilon|$  and  $\Delta t$  should increase together, but there is a large variability in the relationship between the two, at least for periods up to 15 days. A larger  $\Delta t$  does not guarantee a larger  $|\varepsilon|$  in any one instance, only in the mean; and the trend in the mean value of  $|\varepsilon|$  is clear (Table 2). A least squares fit in log-log space gives

$$\text{mean } |\varepsilon| = 0.018 \Delta t^{0.50} \quad (9)$$

**Table 2.** The Magnitude of Ice Deformation  $|\varepsilon|$  As a Function of the Time Interval Over Which That Deformation Is Measured  $\Delta t$

$\Delta t$ , days	Mean $ \varepsilon $	Number of Scenes
3	0.030	848
6	0.046	31
9	0.050	20
12	0.060	8
15	0.070	7

Each value of  $|\varepsilon|$  is an average over the indicated number of scenes.

with a squared correlation of 0.98. The square root dependence of the deformation on the time interval is reminiscent of a two-dimensional random walk process. Dividing through by  $\Delta t$  gives the mean strain rate, and setting  $\Delta t = 30$  days gives a monthly mean strain rate of about 0.33% per day, which is consistent with monthly mean values of the large-scale strain rate invariants computed by optimal interpolation from buoy displacements (R. Moritz, personal communication, 1994). In order to test whether the cavitating fluid model gives a reasonable approximation to monthly data, we would need a large number of scenes showing deformations of  $0.018(30)^{1/2} = 10\%$  or more, or with  $\Delta t$  of the order of 30 days, which we do not have.

## 6. Model Parameterizations of Opening and Closing

### 6.1. Two-Level Models

In models of ice dynamics with two levels of ice thickness, such as those of *Hibler* [1979] and others, the equation for the concentration  $A$  of the thick ice is

$$DA/Dt = -\dot{\epsilon}_1 A + S_A \quad (10)$$

where  $D/Dt$  is the material derivative and  $S_A$  represents the thermodynamic terms. (*Hibler* adds a diffusion term for numerical stability; this does not affect our argument). The divergence of the velocity field  $\dot{\epsilon}_1$  is usually written as  $\nabla \cdot \mathbf{u}$ , but we retain the notation of sections 3–5. The concentration of the thin ice or open water is  $1 - A$ , and (10) implies

$$\frac{D(1-A)}{Dt} = -\dot{\epsilon}_1(1-A) + \dot{\epsilon}_1 - S_A \quad (11)$$

which shows that the open water has a source term,  $\dot{\epsilon}_1$ ; but the data in Figure 6 show that the source term should depend on the shear in the velocity field  $\epsilon_{11}$ , as well as the divergence  $\dot{\epsilon}_1$ . Even when the ice is converging ( $\theta > 90^\circ$ ), there is still some opening of leads. The source term can be generalized to include shear, as follows.

Equations (10) and (11) can be derived in a slightly more general form from the ice thickness distribution equation of *Thorndike et al.* [1975] by integrating it over the appropriate range of thicknesses. The new source term in (11) comes from integrating the redistribution term  $\psi$  in the thickness equation:

$$\psi = |\dot{\epsilon}|[\alpha_o(\theta)\delta(h) + \alpha_r(\theta)w(h, g)] \quad (12)$$

where  $h$  is the ice thickness,  $\delta(h)$  is the Dirac delta distribution,  $w(h, g)$  is a function called the “ridging mode,” and  $g = g(h)$  is the ice thickness distribution. The functions  $\alpha_o(\theta)$  and  $\alpha_r(\theta)$  are the same as those introduced in (4). The  $\psi$  term specifies how ice thickness is redistributed by opening and ridging. The factor  $\delta(h)$  indicates that opening creates ice of zero thickness. The factor  $w(h, g)$  describes the ice involved in ridging: it is the normalized difference between the distribution of ice that ridges and the distribution of the newly ridged ice; its integral over all  $h$  is  $-1$  [*Thorndike et al.*, 1975; *Hibler*, 1980]. Let thin ice have  $h \leq h_0$ , and define

$$W = 1 + \int_0^{h_0} w(h, g) dh. \quad (13)$$

Integrating (12) over the range of thin ice ( $0 \leq h \leq h_0$ ) gives the more general term  $\Psi_{\text{thin}}$  that should replace the source term  $\dot{\epsilon}_1$  in (11):

$$\begin{aligned} \Psi_{\text{thin}} &= \int_0^{h_0} \psi dh = |\dot{\epsilon}|[\alpha_o(\theta) + \alpha_r(\theta)(-1 + W)] \\ &= \dot{\epsilon}_1 + |\dot{\epsilon}|\alpha_r(\theta)W \end{aligned} \quad (14)$$

since  $|\dot{\epsilon}|[\alpha_o(\theta) - \alpha_r(\theta)] = d(\text{opening} - \text{closing})/dt = \dot{\epsilon}_1$ . This implies that an extra term should be added to the right-hand side of (10):

$$\Psi_{\text{thick}} = -|\dot{\epsilon}|\alpha_r(\theta)W. \quad (15)$$

In particular, using the  $\alpha_r(\theta)$  from (8) associated with the elliptical yield curve,

$$\Psi_{\text{thin}} = \dot{\epsilon}_1 + \frac{1}{2}(\Delta - \dot{\epsilon}_1)W \quad \Psi_{\text{thick}} = -\frac{1}{2}(\Delta - \dot{\epsilon}_1)W \quad (16)$$

where  $\Delta = (\dot{\epsilon}_1^2 + \dot{\epsilon}_{11}^2/e^2)^{1/2}$  and  $e$  is the aspect ratio of the elliptical yield curve. (This is the same  $\Delta$  defined by *Hibler* [1979, 1980]). Equation (16) shows how the shear  $\epsilon_{11}$  enters the redistribution term for thick ice ( $\Psi_{\text{thick}}$ ) that should be appended to (10) for the ice concentration  $A$ . The corresponding redistribution term for open water ( $\Psi_{\text{thin}}$ ) is greater than  $\dot{\epsilon}_1$ ; more open water is created than is indicated simply by the net divergence. The special case  $h_0 = 0$  ( $W = 1$ ) gives the largest possible value of  $\Psi_{\text{thin}}$ . If  $W$  is taken to be zero in (14) and (15), as in the standard two-level models, then no source term should be added to (10), and the open water source term is just the divergence  $\dot{\epsilon}_1$ . Notice that this implies a very particular value for  $h_0$ , which would be defined by (13).

The evaluation of  $W$  for the case  $h_0 > 0$  requires a brief digression into the ice thickness distribution theory of *Thorndike et al.* [1975] applied to two-level models. First, the conservation of ice volume in two-level models is enforced through an equation for the mean ice thickness  $\bar{h}$ :

$$D\bar{h}/Dt = -\dot{\epsilon}_1\bar{h} + S_h \quad (17)$$

where  $S_h$  represents the thermodynamic terms. If the thick ice has thickness  $H$ , then  $\bar{h} = (1 - A)(0) + (A)(H)$ , and so  $H = \bar{h}/A$ . The ice thickness distribution  $g(h)$  then consists of two spikes, one for ice of thickness 0 and one for ice of thickness  $H$ :

$$g(h) = (1 - A)\delta(h) + A\delta(h - H). \quad (18)$$

Changes in the areal extent of ice affect the area under the spikes, and changes in the ice thickness affect the location of the second spike. If ridging were allowed, for example, by the inclusion of the term  $\Psi_{\text{thick}}$  (equation (16)) into (10) for the ice concentration, then a ridging event would cause the second spike to move to the right (increasing  $H$ ) and shrink in area (decreasing  $A$ ) in such a way that  $AH = \bar{h} = \text{constant}$ .

Using (18) and following the development of the ridging mode  $w(h, g)$  of *Thorndike et al.* [1975], we find that

$$W = 1 - \int_0^{1-A} b(G) dG \quad (19)$$

where  $b(G)$  is the weighting function that characterizes the range of ice thicknesses that participate in ridging. The function  $b(G)$  is monotone decreasing (thicker ice is less likely to

participate in ridging than thinner ice) and its integral over all  $G$  is 1. *Thorndike et al.* [1975] used the linear form

$$b(G) = \begin{cases} \frac{2}{G^*} \left[ 1 - \frac{G}{G^*} \right] & G \leq G^* \\ 0 & G > G^* \end{cases} \quad (20)$$

where  $G^* = 0.15$  is the fraction below which all ridging occurs. Substituting (20) into (19) leads to

$$W = \begin{cases} \left[ 1 - \frac{1-A}{G^*} \right]^2 & 1-A \leq G^* \\ 0 & 1-A > G^* \end{cases} \quad (21)$$

Finally, referring back to (16), the form of the mechanical redistribution terms  $\Psi_{\text{thin}}$  and  $\Psi_{\text{thick}}$  can be understood as follows. If the concentration of open water ( $1 - A$ ) exceeds the threshold  $G^*$ , then no ridging occurs and  $\Psi_{\text{thick}} = 0$ . If the concentration of open water is less than  $G^*$ , then ridging reduces the areal fraction of thick ice ( $\Psi_{\text{thick}} < 0$ ) and increases the areal fraction of open water by an equivalent amount. The additional source of open water depends on the shear  $\dot{\epsilon}_{11}$  through the term  $\Delta$ , and it depends on the open water concentration through the factor  $W$ .

To give a numerical example, consider the case of pure shear ( $\dot{\epsilon}_1 = 0$ ) and 5% open water. Then  $\Psi_{\text{thin}} = (\dot{\epsilon}_{11}/2e)(2/3)^2$ . With  $e = 2$  and  $\dot{\epsilon}_{11} = 1\%/day$  the source term for open water is about 0.1%/day.

*Hibler* [1984] recognized the need for an additional source of open water due to shearing deformation. (His  $1 - P$  is exactly the same function as our  $W$ .) *Flato and Hibler* [1991] used a weighting function  $b(G)$  proportional to  $e^{-kG}$  (with constant  $k = 20$ ), resulting in  $W = e^{-k(1-A)}$  (their  $K_A$ ). This form was chosen for consistency with their parameterization of the ice strength. In these two papers the redistribution term is  $-(\Delta - |\dot{\epsilon}_1|)W/2$ , which differs from our  $\Psi_{\text{thick}}$  (equation (16)) only by the absolute value around  $\dot{\epsilon}_1$ . Their term was only meant to account for the effect of pure shearing deformations, so it is symmetric with respect to  $\dot{\epsilon}_1$ . Our redistribution term, which is derived from the theory of *Thorndike et al.* [1975], is asymmetric with respect to  $\dot{\epsilon}_1$ , reflecting the fact that less open water would be removed by convergent motion than would be gained by divergent motion of the same magnitude. This is simply due to the interlocking geometry of floes and leads. Of course, a larger and larger force would be required to maintain a constant convergent motion, since the pack ice strengthens with increasing concentration and thickness.

There are two important consequences of the redistribution term in the concentration equation, which we write as  $DA/Dt = -\dot{\epsilon}_1 A + \Psi_{\text{thick}}$  (ignoring the thermodynamic term for this discussion). The first consequence is that more open water is produced than in the standard two-level formulation, because  $\Psi_{\text{thick}}$  is a sink of thick ice, hence a source of open water. This may obviate the need for a minimum lead fraction parameter, which is inserted by some models as a threshold below which the open water concentration is not allowed to fall. In fact, it is exactly the mechanism of open water production through small-scale opening and closing of the ice that the minimum lead fraction is meant to parameterize [*Chapman et al.*, 1994]. The second consequence of the redistribution term is that the ice concentration cannot exceed unity. In the standard two-level model, under sustained convergence it is possible for  $A$  to become bigger than 1. In this case,  $A$  is reset to 1

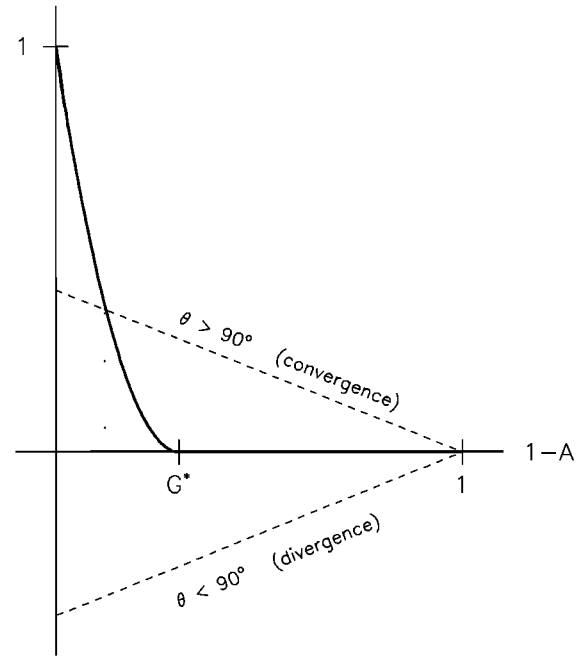


**Figure 7.** Graphical solution of equation (22) for the equilibrium open water concentration,  $1 - A$ , for different types of constant ice deformation characterized by  $\theta$ . The dashed lines represent the left-hand side of (22) for two values of  $\theta$ . The solid curve is the right-hand side of (22) for the function  $W$  given by (21). When  $\theta < 90^\circ$  (divergence), the only solution is  $1 - A = 1$  or no ice. When  $\theta > 90^\circ$  (convergence), the equilibrium open water concentration (vertical dotted line) is between 0 and  $G^*$ .

and the ice thickness is increased instead, to conserve ice volume. This is essentially a redistribution process that turns on when  $A$  reaches 1. *Gray and Morland* [1994] formulated a slightly more general two-level model in which  $A$  approaches 1 asymptotically under sustained convergence, with the rate being controlled by a model function. This function can now be identified with our redistribution term. In addition, we can compute the equilibrium ice concentration under different types of constant ice deformation. Setting  $DA/Dt$  to zero gives  $-\dot{\epsilon}_1 A + \Psi_{\text{thick}} = 0$ . Using  $\dot{\epsilon}_1 = |\dot{\epsilon}| \cos \theta$  and the general form of  $\Psi_{\text{thick}}$  from (15), we have

$$-\frac{\cos \theta}{\alpha_r(\theta)} A = W. \quad (22)$$

Recall that  $W$  depends on  $A$ , as in (21) for example. The left-hand side of (22) is a family of lines with parameter  $\theta$ . Figure 7 shows the solution of (22) for  $A$  (or  $1 - A$ ), in which the left-hand side is plotted with dashed lines for two values of  $\theta$  and the right-hand side is plotted as a solid curve for the  $W$  of (21). When  $\theta < 90^\circ$  (divergence), the only solution is  $1 - A = 1$  or no ice. When  $\theta > 90^\circ$  (convergence), the equilibrium open water concentration (vertical dotted line) is between 0 and  $G^*$ . For example, using the  $\alpha_r(\theta)$  from (8) associated with the elliptical yield curve and the parameter values  $e = 2$ ,  $G^* = 0.15$ , and  $\theta = 135^\circ$  (uniaxial compression), the equilibrium open water concentration is about 0.5%. Under pure convergence ( $\theta = 180^\circ$ ),  $1 - A$  goes to 0, and under pure shear ( $\theta = 90^\circ$ ),  $1 - A$  goes to  $G^*$ .

A two-level model with a redistribution term, such as the

one described here, may be an improvement over the standard two-level model, but it still suffers from the defect that it must reduce the area of thick ice to compensate for the additional open water. However, it is the area of thin ice, not thick ice, that should decrease when ridging and open water production occur. Two-level models do not distinguish between open water and thin ice. Therefore a three-level model consisting of open water, thin ice, and thick ice, with two concentration equations, might provide a more realistic treatment without adding the complication of a full thickness distribution.

## 6.2. A Three-Level Model

Let  $A_1$  and  $A_2$  be the concentrations of thin and thick ice, and let  $A_0 = 1 - A_1 - A_2$  be the concentration of open water. Let  $h_0$  be the thickness that separates open water from thin ice, and let  $h_1$  separate thin ice from thick ice. (Reasonable values might be  $h_0 = 5$  cm and  $h_1 = 50$  cm). The redistribution terms in the equations for  $A_1$  and  $A_2$  are of the form  $\Psi_1 = |\dot{\epsilon}| \alpha_r(\theta) W_1$  and  $\Psi_2 = |\dot{\epsilon}| \alpha_r(\theta) W_2$ , where

$$W_1 = \int_{h_0}^{h_1} w(h, g) dh \quad W_2 = \int_{h_1}^{\infty} w(h, g) dh \quad (23)$$

and  $w(h, g)$  is again the ridging mode. Using the viscous-plastic rheology and the  $\alpha_r(\theta)$  from (8) associated with the elliptical yield curve, the concentration equations for thin and thick ice are then

$$\frac{DA_1}{Dt} = -\dot{\epsilon}_1 A_1 + S_1 + \frac{1}{2}(\Delta - \dot{\epsilon}_1) W_1 \quad (24a)$$

$$\frac{DA_2}{Dt} = -\dot{\epsilon}_1 A_2 + S_2 + \frac{1}{2}(\Delta - \dot{\epsilon}_1) W_2 \quad (24b)$$

where  $S_1$  and  $S_2$  are thermodynamic terms. Extending (18) to the present three-level model, we assume an ice thickness distribution of the form

$$g(h) = A_0 \delta(h) + A_1 \delta(h - H_1) + A_2 \delta(h - H_2) \quad (25)$$

where  $H_1$  and  $H_2$  are the thicknesses of thin ice and thick ice. Following the development of the ridging mode  $w(h, g)$  of *Thorndike et al.* [1975], we can evaluate  $W_1$  and  $W_2$  using the thickness distribution of (25) and the linear weighting function of (20). The result, written in terms of auxiliary functions  $V_1$  and  $V_2$ , is

$$W_1 = -5(V_1 - V_2)/4 \quad W_2 = (V_1 - 5V_2)/4 \quad (26)$$

where (analogous to (21))

$$V_1 = \begin{cases} \left[1 - \frac{A_0}{G^*}\right]^2 & A_0 \leq G^* \\ 0 & A_0 > G^* \end{cases} \quad (27)$$

$$V_2 = \begin{cases} \left[1 - \frac{A_0 + A_1}{G^*}\right]^2 & A_0 + A_1 \leq G^* \\ 0 & A_0 + A_1 > G^* \end{cases}$$

Since  $A_0 = 1 - A_1 - A_2$ , (24a), (24b), and (26) imply that the concentration of open water is governed by

$$\frac{DA_0}{Dt} = -\dot{\epsilon}_1 A_0 + (-S_1 - S_2) + \dot{\epsilon}_1 + \frac{1}{2}(\Delta - \dot{\epsilon}_1) V_1 \quad (28)$$

which shows that the source term for open water is  $\Psi_0 = \dot{\epsilon}_1 + \frac{1}{2}(\Delta - \dot{\epsilon}_1) V_1$ . This term is greater than  $\dot{\epsilon}_1$  when the amount of open water is small ( $A_0 < G^*$ ), because shearing deformation (which enters through the term  $\Delta$ ) also contributes to the creation of open water.

To give a numerical example, suppose  $A_0 = 0.05$ ,  $A_0 + A_1 = 0.15$ , and  $G^* = 0.15$ . Then  $V_1 = 4/9$  and  $V_2 = 0$ , so  $W_1 = -5/9$  and  $W_2 = 1/9$ . For the case of pure shear ( $\dot{\epsilon}_1 = 0$ ) the redistribution terms for open water, thin ice, and thick ice are then  $\Psi_0 = (\dot{\epsilon}_{11}/2e)(4/9)$ ,  $\Psi_1 = (-5/4)\Psi_0$ , and  $\Psi_2 = (1/4)\Psi_0$ . These relationships can be understood in terms of the following hypothetical scenario. Consider a lead covered by thin ice whose area is at least five units. Suppose a new lead forms nearby (within the same material element or grid cell), creating four units of open water and forcing the first lead to close. Four units of the thin ice are piled up into a pressure ridge that occupies one unit of area. The net area change (divergence) of the cell is zero; four units of open water are gained, and five units of thin ice are transformed into one unit of thick (ridged) ice. Under this scenario the standard two-level models would show no open water production and no ridging. A modified two-level model with a redistribution term, as in section 6.1, would give four units of new open water and a loss of four units of thick ice.

Qualitatively, the concentration equations (24a), (24b), and (28) show that deformation of the ice pack is a source of open water through the opening of new leads, and ridging is a sink of thin ice and a source of thick ice. The thermodynamic terms replenish the thin ice by freezing the open water (during winter conditions) and add to the thick ice through continued growth of the thin ice.

To complete the three-level model, we need to specify how the ice thicknesses  $H_1$  and  $H_2$  evolve. Instead of relating  $H_1$  and  $H_2$  to a single average ice thickness, we choose to keep track of these physical thicknesses directly. Their evolution equations are

$$\frac{DH_1}{Dt} = f_1 \quad \frac{DH_2}{Dt} = f_2 + R_2 \quad (29)$$

where  $f_1$  and  $f_2$  are thermodynamic growth rates and  $R_2$  is a term due to ridging. The first part of (29) says that the thickness of a material element of thin ice can only change due to thermodynamic growth and melt. (When thin ice ridges, it is no longer thin ice; this is accounted for by the redistribution terms in the concentration equations, and it does not change the thickness of the remaining thin ice.) The second part of (29) allows the thickness of thick ice to change thermodynamically and mechanically. The term  $R_2$  represents the change in the thickness of thick ice due to the addition of ridged (formerly thin) ice. Conservation of ice volume dictates the form of  $R_2$ . The volume of a material element can only change due to motion, deformation, or ridging. In other words,  $D(A_1 H_1 + A_2 H_2)/Dt$  can only depend on thermodynamic terms. Substituting (24a), (24b), and (29) into this expression and setting the sum of the nonthermodynamic terms equal to zero gives

$$R_2 = \dot{\epsilon}_1 \left[ \frac{A_1 H_1 + A_2 H_2}{A_2} \right] - \left[ \frac{\Psi_1 H_1 + \Psi_2 H_2}{A_2} \right]. \quad (30)$$

This completes the description of the three-level model. We have not specified the form of any of the thermodynamic terms, which is beyond the scope of this work, but we have

indicated where they belong. To summarize, the open water production in the three-level model depends on the shear in the ice pack, as well as the divergence, as indicated by the data. Since the source term for open water is larger than that of standard two-level models, which use only the divergence, there may be no need for a minimum lead fraction or a maximum ice concentration parameter. The redistribution terms are theoretically based;  $|\dot{\epsilon}|_{\alpha_r}(\theta)$  depends on the rheology, and  $W_1$  and  $W_2$  depend on the ridging mode. The three-level model is still simple (it requires only two concentration equations), but it is capable of giving the right qualitative behavior without a full thickness distribution.

## 7. Conclusions

We have used several hundred thousand satellite measurements of sea ice displacement to compute the opening, closing, and deformation of the ice cover. We make the following observations.

1. On a timescale of 3 days the opening and closing can be parameterized quite well in terms of the deformation based on a plastic rheology with an elliptical yield curve (with aspect ratio 2). Certain other yield curves also provide a good fit to the data. This parameterization relates small-scale (several kilometer) lead activity to large-scale (several hundred kilometer) average deformation.

2. On timescales longer than 3 days the average strain rate appears to decay like the reciprocal square root of time. Measurements of sea ice displacement over 30-day time periods with strains of the order of 10% would be required to test the cavitating fluid rheology, which is hypothesized to be appropriate for sea ice models driven by monthly average forcing. The ERS 1 SAR data needed to make these measurements exist.

3. In the parameterization of opening and closing in terms of deformation, the scatter in the data can be attributed to measurement error. It need not necessarily be explained by invoking a random model of ice motion.

4. Sea ice models with two categories or levels of ice thickness can be adapted to account for the effects of shearing and ridging on the open water/thin ice fraction by adding an appropriate redistribution term to the ice concentration equation. This term also prevents the ice concentration from exceeding 1. However, three-level models that distinguish open water from thin ice would be much better suited to the task of treating open water production. We have formulated such a model but have not implemented it numerically.

5. Finally, geophysical processing systems are necessary tools for analyzing large volumes of satellite data in a consistent and timely manner. The next generation of ice-tracking GPS will follow Lagrangian elements of ice and attempt to infer the thickness distribution of thin ice from the time history of area changes and a thermodynamic model [Kwok et al., 1995].

**Acknowledgments.** We thank G. Flato for several informative discussions and reviews. We also thank C. Geiger for helpful comments. This work was performed by H. Stern and D. Rothrock at the Polar Science Center, University of Washington, under grant NAGW-2513

from NASA and under the POLES project, a NASA EOS investigation, grant NAGW-2407; and by R. Kwok at the Jet Propulsion Laboratory, California Institute of Technology, under contract with NASA.

## References

- Chapman, W. L., W. J. Welch, K. P. Bowman, J. Sacks, and J. E. Walsh, Arctic sea ice variability: Model sensitivities and a multidecadal simulation, *J. Geophys. Res.*, **99**, 919–935, 1994.
- Fetterer, F., D. Gineris, and R. Kwok, Sea ice type maps from Alaska Synthetic Aperture Radar Facility imagery: An assessment, *J. Geophys. Res.*, **99**, 22,443–22,458, 1994.
- Fily, M., and D. A. Rothrock, Opening and closing of sea ice leads: Digital measurements from synthetic aperture radar, *J. Geophys. Res.*, **95**, 789–796, 1990.
- Flato, G. M., and W. D. Hibler III, An initial numerical investigation of the extent of sea-ice ridging, *Ann. Glaciol.*, **15**, 31–36, 1991.
- Flato, G. M., and W. D. Hibler III, Modeling pack ice as a cavitating fluid, *J. Phys. Oceanogr.*, **22**, 626–651, 1992.
- Flato, G. M., and W. D. Hibler III, Ridging and strength in modeling the thickness distribution of Arctic sea ice, *J. Geophys. Res.*, **100**, 18,611–18,626, 1995.
- Gray, L. M. N. T., and L. W. Morland, A two-dimensional model for the dynamics of sea ice, *Philos. Trans. R. Soc. London A*, **347**, 219–290, 1994.
- Hibler, W. D., III, A dynamic thermodynamic sea ice model, *J. Phys. Oceanogr.*, **9**, 815–846, 1979.
- Hibler, W. D., III, Modeling a variable thickness sea ice cover, *Mon. Weather Rev.*, **108**, 1943–1973, 1980.
- Hibler, W. D., III, The role of sea ice dynamics in modeling CO<sub>2</sub> increases, in *Climate Processes and Climate Sensitivity*, *Geophys. Monogr. Ser.*, vol. 29, edited by J. E. Hansen and T. Takahashi, pp. 238–253, Washington, D. C., 1984.
- Holland, D. M., L. A. Mysak, D. K. Manak, and J. M. Oberhuber, Sensitivity study of a dynamic thermodynamic sea ice model, *J. Geophys. Res.*, **98**, 2561–2586, 1993.
- Kwok, R., J. C. Curlander, R. McConnell, and S. S. Pang, An ice-motion tracking system at the Alaska SAR Facility, *IEEE J. Oceanic Eng.*, **15**, 44–54, 1990.
- Kwok, R., E. Rignot, and B. Holt, Identification of sea ice types in spaceborne synthetic aperture radar data, *J. Geophys. Res.*, **97**, 2391–2402, 1992.
- Kwok, R., D. A. Rothrock, H. L. Stern, and G. F. Cunningham, Determination of the age distribution of sea ice from Lagrangian observations of ice motion, *IEEE Trans. Geosci. Remote Sens.*, **33**, 392–400, 1995.
- Maykut, G. A., Energy exchange over young sea ice in the central Arctic, *J. Geophys. Res.*, **83**, 3646–3658, 1978.
- Rothrock, D. A., The energetics of the plastic deformation of pack ice by ridging, *J. Geophys. Res.*, **80**, 4514–4519, 1975.
- Thorndike, A. S., Kinematics of Sea Ice, in *The Geophysics of Sea Ice*, *NATO ASI Ser. B*, vol. 146, edited by N. Untersteiner, chap. 7, pp. 489–549, Plenum, New York, 1986.
- Thorndike, A. S., A random discontinuous model of sea ice motion, *J. Geophys. Res.*, **92**, 6515–6520, 1987.
- Thorndike, A. S., D. A. Rothrock, G. A. Maykut, and R. Colony, The thickness distribution of sea ice, *J. Geophys. Res.*, **80**, 4501–4513, 1975.
- Walsh, J. E., and H. J. Zwally, Multiyear sea ice in the Arctic: Model- and satellite-derived, *J. Geophys. Res.*, **95**, 11,613–11,628, 1990.
- R. Kwok, Jet Propulsion Laboratory, California Institute of Technology, 4800 Oak Grove Drive, Pasadena, CA 91109.  
D. A. Rothrock and H. L. Stern, Polar Science Center, University of Washington, 1013 N.E. 40th Street, Seattle, WA 98105. (e-mail: harry@apl.washington.edu)

(Received November 10, 1994; revised June 16, 1995; accepted July 24, 1995.)